Journal of Molecular Catalysis A: Chemical 350 (2011) 56–63

Contents lists available at SciVerse ScienceDirect

Journal of Molecular Catalysis A: Chemical

journal homepage: www.elsevier.com/locate/molcata

Facile fabrication of nanostructured Pd–Fe bimetallic thin films and their electrodechlorination activity

Cuicui Qiu[a], Xiaoqiang Dong[b], Minghu Huang[c], Sihui Wang[a], Houyi Ma[a,d,*]

[a] Key Laboratory for Colloid and Interface Chemistry of State Education Ministry, School of Chemistry and Chemical Engineering, Shandong University, Jinan 250100, China
[b] Sinopec Research Institute of Petroleum Engineering, Beijing 100101, China
[c] School of the Ocean, Harbin Institute of Technology at Weihai, Weihai 264209, China
[d] Beijing National Laboratory for Molecular Science, Beijing 100190, China

ARTICLE INFO

Article history:
Received 18 June 2011
Received in revised form 4 September 2011
Accepted 8 September 2011
Available online 16 September 2011

Keywords:
Palladium
Iron
Bimetallic film
Electro-dechlorination activity
Carbon tetrachloride (CT)

ABSTRACT

A series of nanostructured Pd–Fe bimetallic thin films with the performance of fast and high-efficiency electrochemical reductive dechlorination were directly formed on glassy carbon electrodes (GCEs) through galvanic replacement of partial Fe^0 nanoparticles by Pd(II) ions. The composition and morphology of such Pd–Fe thin films are strongly dependent on the sacrificial Fe film templates fabricated by a template-free, double-potential step electrodeposition technique. The size, shape and morphology of the Fe nanoparticles that constitute the Fe thin films can be controlled well by adjusting the concentration of Fe^{2+} ions in electrolyte solutions. Due to the good synergistic effect between Pd and Fe, the as-prepared Pd–Fe thin films with the novel microstructure display a high reactivity towards the electrochemical reductive dechlorination of carbon tetrachloride (CT), which closely related to the composition of Pd–Fe thin films, applied potential and temperature. The dechlorination reaction of CT complied with pseudo-first-order kinetics.

1. Introduction

Many chlorinated organic compounds (COCs), such as carbon tetrachloride (CT), trichloroethylene (TCE), and other organochlorine contaminants listed at the Stockholm Convention on Persistent Organic Pollutants (2001), are highly toxic, persistent and bioaccumulative. Once discharged into the environment, a great threat will be posed to human heath and ecological environment [1,2]. Although it has been abandoned in extinguishing systems and refrigeration equipments due to its potential hazard to ozone depletion [3], CT is still widely used as a solvent in chemical plants and labs at the present time, which leads to huge amounts of residues in groundwater or in public water systems [4,5]. It is very urgent to develop effective methods of converting COCs to nontoxic or less toxic nonchlorinated analogues. An effective means to eliminate COCs is to remove the elemental chlorine by converting organic chlorine into inorganic chloride ions, which occurs with the formation of nontoxic or low-toxic parent hydrocarbon compounds [6,7].

Much effort has been devoted to the degradation of COCs, but most of the dechlorination methods (e.g. activated carbon adsorption, physical separation, and photocatalytic oxidation) are limited in advanced water treatment due to the high cost and especially the formation of secondary intractable contaminants. The distinguished features of electrochemical dechlorination methods include rapid reaction rate, mild reaction conditions, low apparatus cost, and especially the green processing technology that does not need additional chemical additives [8].

Though during the past decade, due to abound resources, low cost and considerable activity, zero-valent iron (ZVI or Fe^0), especially nano-Fe [9,10], was widely used as a potent electron donor or reductant for the hydrodechlorination of COCs, it should be noted that the practical application of Fe in the dechlorination of COCs has been considerably limited due to its intrinsic defects [11]. It is of interest that these disadvantages can be efficiently eliminated when using Fe-based bimetallic materials (e.g. Fe/Pd [12,13], Fe/Ni [14,15], Fe/Al [16], Fe/Au [17], Fe/Pt [11]) as substitutes for monometallic Fe^0. The incorporation of the lower hydrogen overpotential metals (e.g. Pd, Pt, etc.) not only increases the density of surface reactive sites, but also prevents the corrosion products from accumulating at the reactive sites on the Fe^0 surface. Because of outstanding adsorbing/absorbing hydrogen capacity under ambient condition, Pd is considered to be one of the most effective hydrodechlorination catalysts [18–20]. Moreover, the combination of Pd and Fe makes it possible to prepare high performance dechlorination catalysts. The existing studies have demonstrated that the Pd–Fe bimetallic catalysts exhibit the higher dechlorination activity [17,21] than other bimetallic catalysts. In view of this, the aim of our

* Corresponding author. Tel.: +86 531 88364959; fax: +86 531 88564464.
E-mail address: hyma@sdu.edu.cn (H. Ma).

1381-1169/$ – see front matter © 2011 Elsevier B.V. All rights reserved.
doi:10.1016/j.molcata.2011.09.004

Table 1
The effect of Fe^{2+} concentration on the composition[a], EASA[b] and RE for electrochemical reductive dechlorination of CT in H_2SO_4 solutions on the Pd–Fe thin films. (For removal efficiency test: potential: −0.2 V; time: 30 min; temperature: 303 K.)

Fe^{2+} concentration (mM)	Pd/Fe weight ratio	Pd/Fe atomic ratio	EASA	RE (%)
5	99.75/0.25 = 399	99.52/0.48 ≈ 207.3	0.33	84.0
10	85.49/14.51 ≈ 5.9	75.52/24.48 ≈ 3.1	0.44	97.4
15	83.03/16.97 ≈ 4.9	71.98/28.02 ≈ 2.6	0.53	51.9
25	18.31/81.69 ≈ 0.2	10.52/89.48 ≈ 0.1	1.70	40.7

[a] The compositions of as-prepared bimetallic films were determined according to EDS analyses.
[b] EASA of Pd–Fe bimetallic thin films was calculated by means of oxygen adsorption method.

paper is to design and fabricate high performance Pd–Fe bimetallic dechlorination catalysts using double-potential step electrodeposition and galvanic replacement methods. Taking electrochemical reductive dechlorination of CT as the research object, we investigated the removal efficiencies of the as-prepared bimetallic Pd–Fe nanocatalysts under different conditions. The present study will provide a new path to fabricate low-temperature high-efficiency nanocatalysts for the dechlorination of COCs. The obtained results are also of fundamental importance to give an in-depth understanding of reductive dechlorination mechanism of COCs on the Pd–Fe bimetallic catalysts.

2. Experimental

All reagents were of AR grade and were used as received from Sinopharm Chemical Reagent Co., Ltd. (Shanghai, China). All of the aqueous solutions were prepared with ultrapure water (>18 MΩ cm). The glassy carbon electrodes (GCEs, ϕ = 4 mm) were used as substrate electrodes. Before each experiment, a GCE was firstly ground with emery papers of decreasing particle sizes to #3500 finish, and then polished with 0.05 μm alumina slurry. Subsequently, the electrode was cleaned ultrasonically in HNO_3 (1:1), washed with ultrapure water, and finally rinsed with ethanol.

Bulk Fe electrode was made from 99.99% pure Fe wire (ϕ = 2.0 mm). The Fe wire was embedded in epoxide resin mould, leaving its cross-section only exposed to the electrolytic solutions. The bulk Fe electrode was treated with the similar procedure used for GCEs except it was not cleaned ultrasonically in HNO_3.

The nanostructured Fe thin films were directly fabricated on GCE substrates (denoted as Fe/GCE) by a double-potential step electrodeposition in a solution of 250 mM NaCl + $FeCl_2$ (with different concentrations) at 303 K. The concentration of $FeCl_2$ was selected as 5, 10, 15, and 25 mM, respectively. All Fe films were prepared by applying two potential pulses in succession: a negative reducing nucleation pulse (−1.15 V) for 1 s and a growth pulse (−1.05 V) for 1000 s. The potentials were controlled by a computer-controlled electrochemical workstation (CHI 650A). Assuming identical faradaic efficiency for the deposition process, the amount of Fe deposited can be estimated by integrating the charge needed to reduce Fe^{2+} ions.

Bimetallic Pd–Fe thin films were prepared by dropping 25 μL of 10 mM acidic solution containing noble metal precursor (H_2PdCl_4) onto the Fe films for 30 min. Seeing that the standard redox potentials of $PdCl_4^{2-}$/Pd and Fe^{2+}/Fe relative to the standard hydrogen electrode (SHE) are +0.951 V and −0.440 V, respectively, the deposition of noble metal Pd onto the surface of Fe thin films occurred through the following galvanic replacement reaction:

$$Fe^0 + PdCl_4^{2-} \rightarrow Fe^{2+} + Pd^0 + 4Cl^- \quad (1)$$

After thoroughly rinsing with ultrapure water, the GCEs modified with the as-prepared Pd–Fe thin film (abbreviated to Pd–Fe/GCE) were placed in 0.5 M H_2SO_4 for carrying out the potential cycling in the designated potential range.

All electrochemical measurements were performed in a conventional three-electrode cell with a CHI 650A electrochemical workstation. The GCEs modified with monometallic Fe or bimetallic Pd–Fe thin films were selected as working electrodes. A bright Pt plate (1.0 cm × 2.0 cm) and a saturated calomel electrode (SCE) were selected as the counter electrode and the reference electrode, respectively. In this paper, the potentials were all referred to the SCE. The reference electrode was led to the surface of the working electrode through a Luggin capillary. The electrolyte solutions were deaerated by bubbling N_2 through the solutions for 10 min before electrochemical tests, and a blanket of N_2 was maintained during electrochemical measurements. Electrochemical reductive dechlorination of CT on the nanostructured Pd–Fe thin films was studied by cyclic voltammetry and potentiostatic electrolysis in 0.5 M H_2SO_4 containing 30 mg L^{-1} CT solutions at different temperatures.

As a complicated reaction for CT dechlorination, the formation of various possible intermediates and products (e.g. CO_2, CO and $HCOO^-$) leads to the measurement difficulty, usually causing a low total carbon mass balance in analysis [22]. In the current study, only the change of CT concentration was analyzed to investigate the dechlorination performance of Pd–Fe bimetallic catalysts. The concentration of CT in the electrolytes before and after potentiostatic electrolysis was analyzed by gas chromatography/mass spectrometry (GC/MS)-QP2010. The gas chromatography was equipped with a DB-5 MS capillary column (30 m × 0.25 mm, 0.25 μm thickness). The column temperature was maintained at 308 K, while the temperature of injection port and ion-trap detector was 473 K. Ultra-pure He was used as the carrier gas at a flow rate of 1.1 mL min^{-1} and a split ratio of 60:1. Before each GC/MS testing, the CT samples were placed in thermostatic water bath at 313 K for 1 h. The change of CT concentration in the solutions before and after potentiostatic electrolysis can be used to determine the removal rates of carbon tetrachloride. Removal efficiency (RE) was calculated as the ratio of the decrease of CT concentration to the initial CT concentration (i.e. RE (%) = $(1 - C/C_0) \times 100$), where C denotes the concentration of CT after electrolysis, and C_0 is the initial concentration of CT).

Structure and surface morphology of Fe films and bimetallic Pd–Fe films were observed by field emission scanning electron microscope (FESEM, JEOL JSM-6700F). The composition of these bimetallic films was analyzed by INCAX-sight energy dispersive X-ray spectrometer equipped on the FESEM. The weight ratios and atomic ratios of Pd to Fe in different bimetallic films were listed in Table 1.

3. Results and discussion

3.1. Preparation of nanostructured Pd–Fe bimetallic thin films and their surface morphology

Herein nanostructured Fe thin films were first electrodeposited onto the GCE substrate by a double-potential step electrodeposition method. From the cyclic voltammograms (CVs) for the voltammetric deposition of Fe shown in Fig. 1(a), it is found that the Fe electrodeposition started at ∼−1.0 V and gave a characteristic cathodic peak centered on −1.13 V during the first negative-going

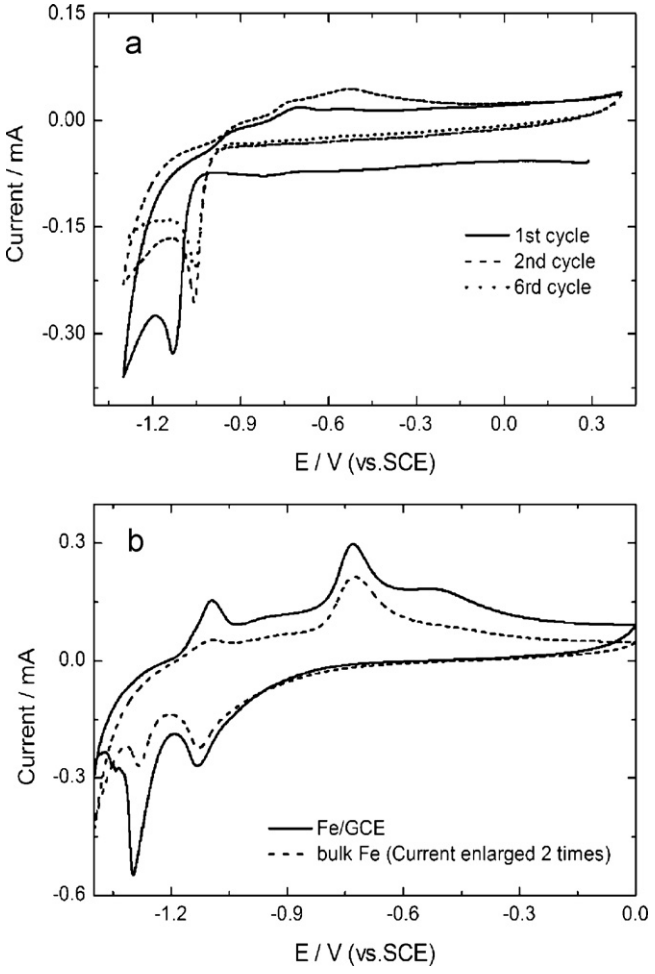

Fig. 1. CVs of (a) GCE in 250 mM NaCl + 10 M $FeCl_2$ mixed solution and (b) Fe/GCE and bulk Fe in 1.0 M KOH solution. Scan rate: 50 mV s^{-1}.

potential scan. However, both the onset potential and cathodic peak potential of the Fe deposition shifted positively by about 100 mV from the second cycle onwards and remained unchanged thereafter. The similar results were reported previously [23,24]. The present voltammetric behavior indicates that Fe deposition process tended to nucleate at a more negative potential on a foreign substrate. Once a monolayer of Fe film formed on the GC substrate, the subsequent deposition on the Fe film became easier, which can be reflected from the significant positive-shift of reduction peak potential. With the increase of potential cyclic number, more Fe nuclei formed on the GC substrate or on the previously formed Fe monolayer, which led to the progressive growth of Fe particles. The deposition of Fe on GCE is a heterogeneous nucleation process, and the Fe "island" forms through a Volmer–Weber growth mode [23,25]. As expected, when selecting −1.15 V and −1.05 V as nucleation potential and nuclear growth potential, respectively, the nano/submicron Fe thin films with hierarchical architectures on the GC substrate were obtained.

CVs of the Fe film modified GCE (Fe/GCE) electrode and the bulk Fe one in 1.0 M KOH solution are shown in Fig. 1(b). As is well known, the oxidation and passivation processes of Fe electrode will take place in alkaline solutions under applied anodic potentials, resulting in the formation of Fe oxide multilayers. The CVs of the bulk Fe electrode display two pairs of current peaks in potential range between −1.4 V and 0 V. Two oxidation peaks appeared near −1.1 V and −0.73 V in the anodic scan, and their corresponding reduction peaks were observed respectively at ∼−1.3 V and −1.13 V in the subsequent cathodic scan. The anodic process involves electrooxidation of Fe^0 into Fe(II) and Fe(III) species.

$$Fe + 2OH^- \rightarrow Fe(OH)_2 + 2e^- \quad (2)$$

$$Fe(OH)_2 + OH^- \rightarrow FeOOH + H_2O + e^- \quad (3)$$

The CVs of the Fe/GCE present similar features to those of the bulk Fe electrode, thereby confirming the formation of Fe thin films on the GC substrate. Besides, it is observed that the hydrogen evolution reaction was decreased obviously on the Fe/GCE as compared to that on the bulk Fe, because no rapid increase in the cathodic current took place at ∼−1.32 V on the Fe/GCE.

Fig. 2 shows SEM images (Fig. 2(a)–(e)) and EDS spectrum (Fig. 2(f)) of the as-prepared Fe thin films fabricated onto the GC substrate. The obvious peaks for Fe in Fig. 2(f) indicate the existence of Fe element. On the other hand, the SEM observations demonstrate that the as-prepared Fe films are not a monolayer film but probably composed of bilayer films. From Fig. 2(d) and its inset, it can be seen that the bottom layer with some irregular structures is a compact thin film composed of quantities of nanoparticles, whereas the surface layer consists of submicron-scale Fe particles that adhere to the bottom layer. The surface morphology of the Fe thin films, especially the shape of large Fe particles in the surface layer, can be regulated conveniently by changing the concentration of Fe^{2+} in the electrolytic solutions. When the concentration of Fe^{2+} was relatively low, most of surface particles adopted a perfect cubic shape. These large particles were scattered on the bottom layer and their particle size was about 130–170 nm, as indicated by a large-scale SEM image (Fig. 2(a)) and an enlarged SEM image (Fig. 2(b)). At a relatively low concentration of Fe^{2+} ions (e.g. 5 mM), a small number of nuclei generated by the electrocrystallization tended to homogenously and slowly grow along ⟨1 0 0⟩, ⟨0 1 0⟩ and ⟨0 0 1⟩ directions, thereby forming regular nanocubes. As the Fe^{2+} ion concentration increased, the surface Fe particles became uneven in the shape and in size (see Fig. 2(c)–(e)). The vast majority of large Fe particles in the surface layer were submicron-scale irregular polyhedra. This phenomenon seemed more evident in the case of 25 mM. In this case, the nuclei were inclined to quickly and heterogeneously grow. At the same time, the number of surface Fe particles increased significantly since the density of nuclei increased with the increasing Fe^{2+} ion concentration [24]. The high coverage of surface particles made the bottom layer of Fe thin films not to be seen, as indicated by Fig. 2(e).

The nanostructured Pd–Fe bimetallic thin films could be fabricated on the GC substrate by using the nanostructured Fe thin films as the sacrificial templates to react with the H_2PdCl_4 solutions. Fig. 3(a)–(d) show typical SEM images for a series of Pd–Fe thin films obtained by galvanic replacement of Fe films with Pd. The surface morphology of the bimetallic thin films strongly depended on that of the sacrificial Fe templates, more exactly on the concentration of Fe^{2+} ions used to prepare the Fe film templates. When the concentration of Fe^{2+} ions increased from 5 mM to 25 mM, the morphology of the bimetallic Pd–Fe films changed from individual particles to submicron-scale flower-shaped particles depending on the significant change in the topography of Fe film templates. The higher the concentration of Fe^{2+}, the rougher the surface morphology of Pd–Fe bimetallic films seemed. The rougher surface structure can provide larger electrochemical active surface area (EASA) of Pd components in the bimetallic thin films (see Table 1), which were determined by means of the oxygen adsorption method [26]. The appearance of both Pd and Fe peaks in the EDS spectrum (Fig. 3(e)) has evidence that the as-prepared films were bimetallic Pd–Fe thin films. The present bimetallic thin films are expected to be in favor of the dechlorination reaction of COCs. The combination of electrodeposition and galvanic replacement enables us to design and fabricate the bimetallic Pd–Fe thin films with controllable morphologies,

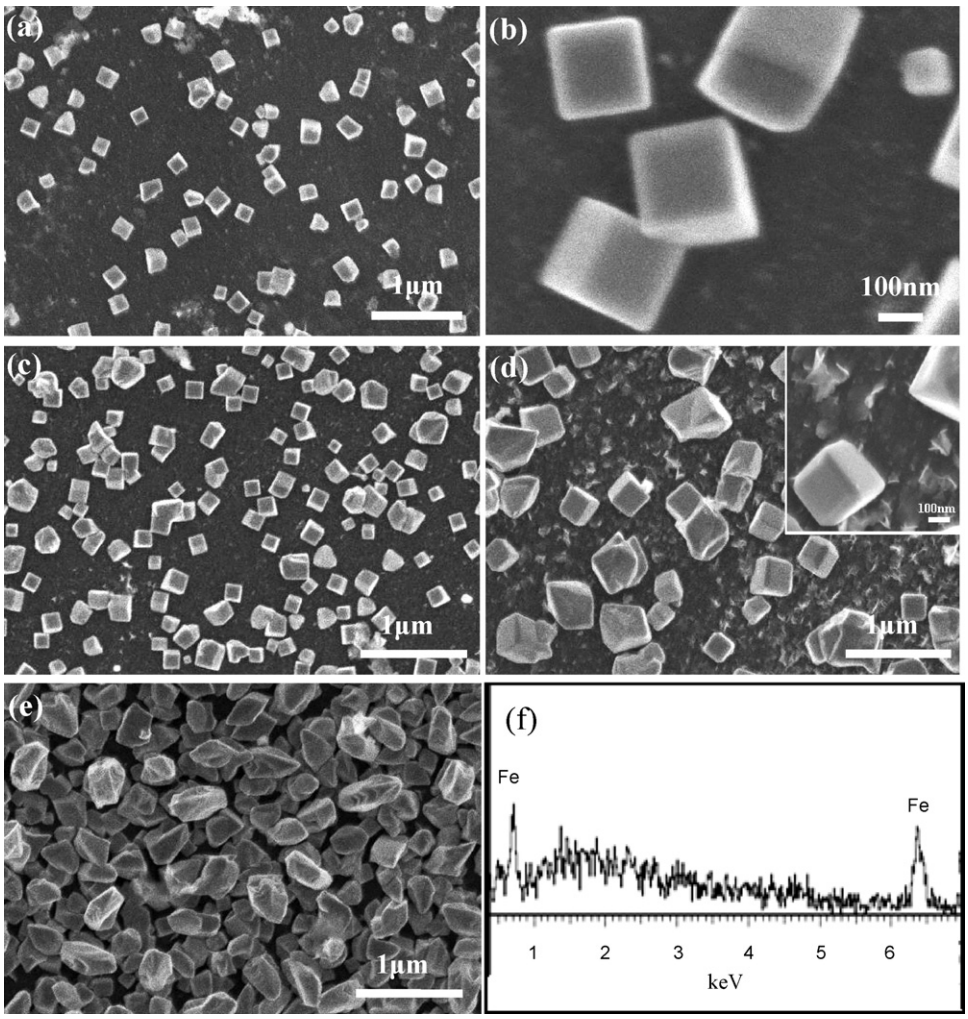

Fig. 2. SEM images and EDS spectrum of the Fe thin films electrodeposited onto GCE substrates in electrolyte solutions with different Fe^{2+} concentrations: (a) 5 mM, (b) 5 mM, (c) 10 mM, (d) 15 mM, (e) 25 mM, and (f) EDS of Fe thin films.

which is more suited to acting as the cathode catalyst materials for electrochemical dechlorination reactions than the Pd–Fe nanoparticles. The microstructure and morphology of the Pd–Fe thin films can be tailored by choosing the Fe film templates or changing the replacement reaction time. The same is true of the composition of the Pd–Fe thin films.

3.2. Electrochemical behavior of Pd–Fe thin films in acidic solutions

3.2.1. Voltammetric behavior of Pd–Fe thin films in acidic solutions

CVs of a GCE covered with the Pd–Fe thin films (Pd–Fe/GCE for short) in 0.5 M H_2SO_4 solutions with and without CT are shown in Fig. 4(a). The CVs obtained in the CT-free solution are basically similar to those of the nanostructured Pd thin films in H_2SO_4 solution [27]. In the hydrogen region, the CVs give two pairs of redox peaks: the two large peaks at the more negative potentials are attributed to the hydrogen evolution and the desorption of absorbed hydrogen respectively, whereas the two small ones at the more positive potentials are associated with the hydrogen adsorption/desorption. The adsorbed hydrogen exists in the form of atomic hydrogen on the Pd surface, which is the stronger reductant for the dechlorination of COCs than the absorbed hydrogen embedded in the Pd lattice. The great change of CV profile in the presence of CT exemplifies the difference in the dechlorination reactivity between absorbed and adsorbed hydrogen. It is observed that, the hydrogen evolution and the hydrogen adsorption were inhibited considerably due to the reaction between adsorbed hydrogen and the adsorbed CT. And the redox peaks associated with the hydrogen adsorption/desorption completely disappeared in the CT-containing solution. Accordingly, the use of Pd–Fe/GCE provides the great possibility to study the effect of different types of hydrogen on electrochemical reductive dechlorination of CT.

3.2.2. Galvanic corrosion of Pd–Fe bimetallic films in acidic solutions

It is known that a galvanic cell is formed when two dissimilar metals are connected electrically while both are immersed in an electrolyte solution and the corrosion rate depends on the surface reaction of both metals. In the Pd–Fe bimetallic system, Pd serves as the cathode in the galvanic cell and the H_2 produced from the Fe^0 corrosion is transferred to the Pd surface, since Pd^0 has the low hydrogen overpotential and the high exchange current density for H^+/H_2. The galvanic effect can accelerate the electron transfer from the corroding Fe^0 to the Pd^0, which is helpful to reduce the accumulation of corrosion intermediates over the Fe surface and further increase the efficiency of hydrogen utilization. It is obvious that the galvanic corrosion of Pd–Fe bimetallic system can enhance the dechlorination rate of COCs as compared with single Fe^0 or Pd^0

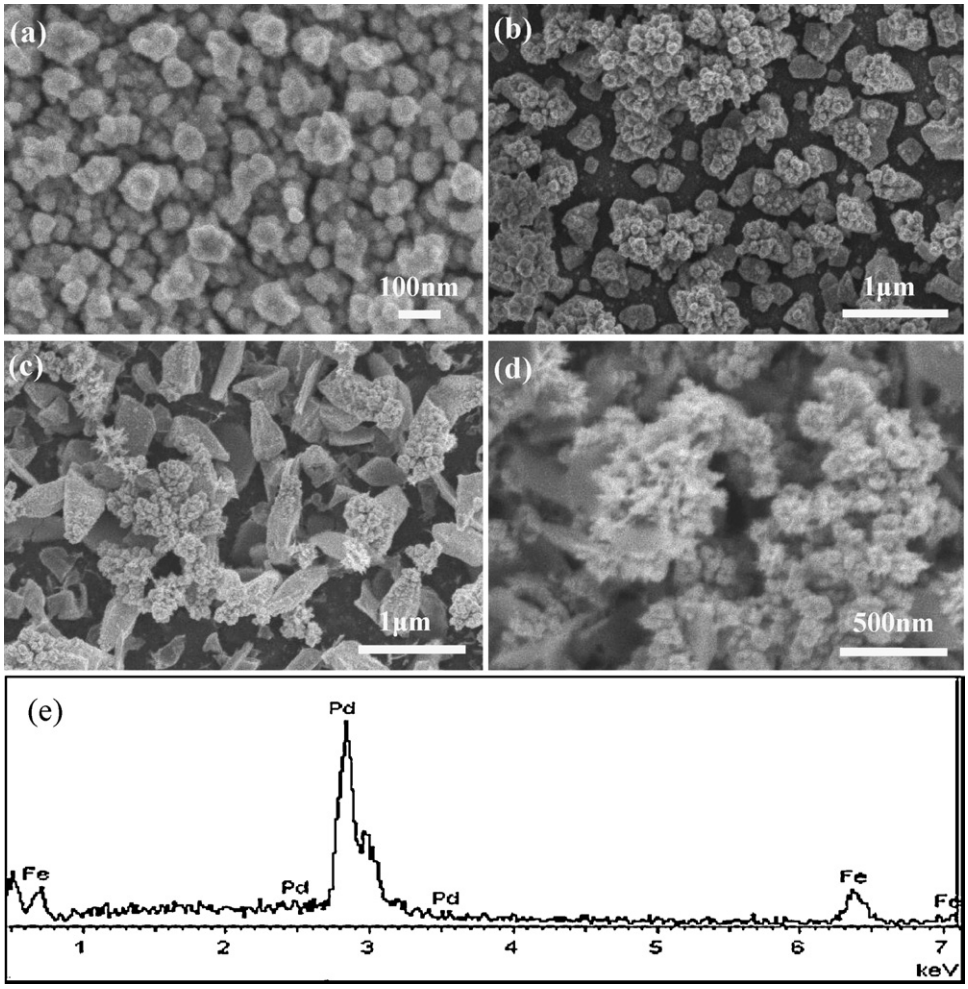

Fig. 3. SEM images and EDS spectrum of the Pd–Fe bimetallic thin films. The Fe film templates were prepared in electrolyte solutions containing different concentrations of Fe^{2+} ions: (a) 5 mM, (b) 10 mM, (c) 15 mM, and (d) 25 mM.

catalyst. This is the main reason that many researchers incorporate a noble metal with low hydrogen overpotential, such as Pd, into Fe^0 nanoparticles [14,28]. The dechlorination mechanism of COCs on the Pd–Fe can be expressed as follows [12,29]:

$$\begin{aligned} &Fe + 2H^+ \rightarrow Fe^{2+} + H_2 \\ &Fe + RCl + H^+ \rightarrow RH + Fe^{2+} + Cl^- \end{aligned} \quad (I)$$

$$\begin{aligned} &2H^+ + 2e^- \leftrightarrow 2H_{ad} \leftrightarrow H_2 \\ &Pd + H_2 \rightarrow Pd \cdot H_2 \\ &Pd + RCl \rightarrow Pd\cdots Cl\cdots R \end{aligned} \quad (II)$$

$$Pd \cdot H_2 + Pd\cdots Cl\cdots R \rightarrow RH + H^+ + Cl^- + 2Pd \quad (III)$$

Fig. 4(b) shows the steady-state curves for the freshly prepared Pd–Fe/GCE in H_2SO_4 solutions with and without CT. Firstly, it can be estimated from the steady-state curve of the Pd–Fe/GCE in the blank solution that the open-circuit corrosion potential of the Pd–Fe thin films is ~0.54 V (vs. SCE), about 1.0 V more positive than that of bulk Fe electrode (<−0.5 V vs. SCE) under the identical conditions. Theoretically, the Fe components of Pd–Fe films have been passivated at such a high positive potential [30]. The driving force for the strong positive-shift of the corrosion potential is the quite high exchange current density of H^+/H_2 on Pd micro-cathodes. The cathodic Tafel slope of 116.1 mV dec^{-1} and anodic Tafel slope of 101 mV dec^{-1}, while in CT-containing solution, the open-circuit potential (OCP) shifted about 20 mV to negative direction and the corrosion current decreased significantly, accompanied by the great change in anodic Tafel slope (63.4 mV dec^{-1}) and little change in the cathodic Tafel slope (116.3 mV dec^{-1}). Besides, in CT-containing solution, a new redox couple was observed around 0.38 V from the measured polarization curve. It is inferred that the oxidation–reduction reaction is related to the dechlorination reaction between CCl_4 and Fe(II) oxides.

3.3. Catalytic activity of Pd–Fe thin films towards the dechlorination of CT

3.3.1. Effect of applied potentials

Now we focused on investigating catalytic activity of Pd–Fe thin films towards the CT dechlorination under different cathodic potentials.

Electrochemical reductive dechlorination of CT was performed in potentiostatic mode. The reaction was controlled at 303 K and was kept for 30 min. Several representative cathodic potentials, −0.05 V (the adsorption of hydrogen occurred), −0.08 V (a monolayer of adsorbed hydrogen formed), −0.1 V (hydrogen started to enter into Pd lattices), −0.15 V (the Pd α-hydride phase formed), −0.2 V (the β-hydride phase formed and hydrogen started to evolve on the electrode surface) [31], were selected to study the effect of different types of hydrogen on removal efficiency of CT. From the data listed in Table 2, it can be found that the adsorbed hydrogen at −0.08 V display a high dechlorination activity, and the

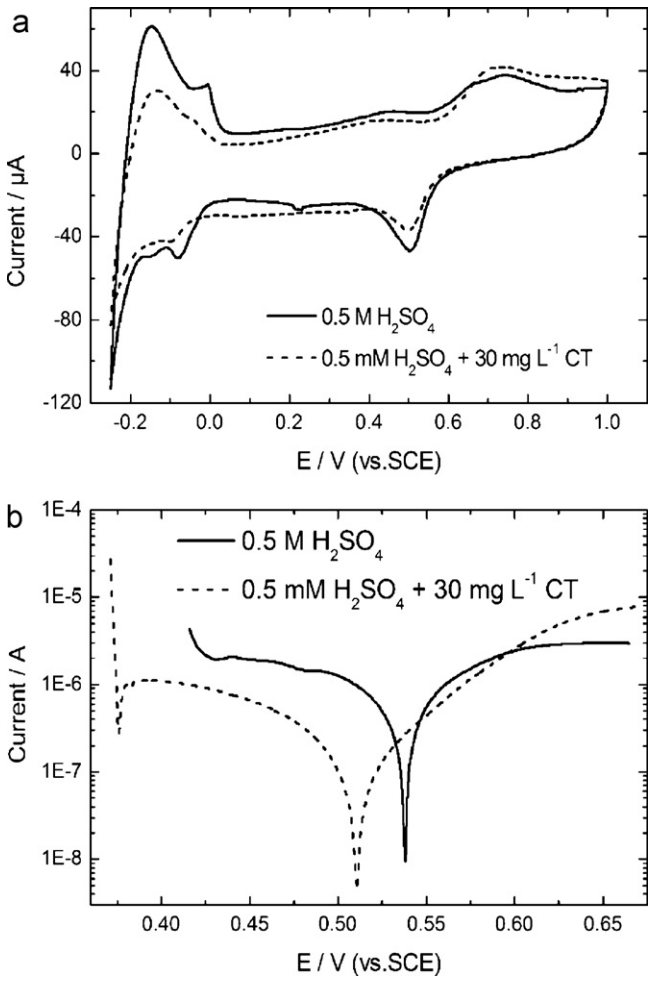

Fig. 4. CVs (a) and Tafel polarization curves (b) of Pd–Fe/GCE in 0.5 M H_2SO_4 with and without 30 mg L^{-1} CT. Scan rate of CVs: 50 mV s^{-1}.

removal efficiency of CT calculated at the potential reached 91.3%, only slightly lower than that (97.4%) obtained at −0.2 V in the case of hydrogen evolution. However, the removal efficiency of CT at −0.15 V was relatively low (39%). The similar phenomenon was observed for the electrochemical reductive dechlorination of CT on nanostructured Pd thin films [27]. The Pd surface was covered by adsorbed-H atoms at −0.08 V, which was advantageous to the surface reaction between H atoms and adsorbed CT molecules, thereby leading to the relatively high removal efficiency. However, as the potential became more negative, H atoms started to permeate into the Pd lattices, forming the Pd α-hydride phase. Because of lack of active adsorbed-H, the CT removal efficiency was lower than that at −0.08 V. The change of removal efficiency with the applied potentials can be interpreted based on the voltammetric behavior of the Pd–Fe thin films. In CT-free H_2SO_4 solutions, a monolayer of hydrogen atoms already occupied the whole Pd surface at −0.15 V. At the moment, there were few active sites on the surface of bimetallic catalysts available for chemisorption of CT. Considering that the surface concentration of metal chloride formed through the chemisorption of CT was quite low, the removal efficiency of CT was naturally relatively low in this case. Nevertheless, this situation was changed at the more negative potentials (e.g. −0.2 V). The adsorbed hydrogen began to desorb from the Pd sites because of the onset of the HER; CT molecules were therefore able to adsorb on the electrode surface and form enough metal chloride. In addition, the evolving hydrogen was able to react with the adsorbed CT molecules at the electrode/solution interface. Consequently, the electrocatalytic hydrogenation (ECH) of CT was promoted significantly, and correspondingly the removal efficiency of CT increased again and even reached a higher value.

Table 2
The RE and E_a for electrochemical reductive dechlorination of CT at different applied cathodic potentials on the Pd–Fe thin films in H_2SO_4 solutions. (Pd/Fe weight ratio: 5.9; for removal efficiency test, time: 30 min; temperature: 303 K.)

Potential (V)	RE (%)	E_a (KJ mol^{-1})
−0.05	52.1	49.1
−0.08	91.3	24.4
−0.1	59.4	39.0
−0.15	39.0	51.0
−0.2	97.4	23.7

3.3.2. Effect of the Pd–Fe ratios in bimetallic thin films

For galvanic corrosion of as-prepared Pd–Fe thin film electrode in acidic solutions, the larger the Pd/Fe area ratios, the faster the corrosion rate of Fe components. The large Pd/Fe area ratio is favorable for increasing dechlorination efficiency of COCs on the Pd-Fe bimetallic catalysts from the point of view of accelerating iron corrosion. But on the other hand, the galvanic corrosion can also cause the passivation of Fe components, which is disadvantageous to the dechlorination of COCs. Therefore, both positive and negative effects of galvanic corrosion on catalytic dechlorination activity of the Pd–Fe bimetallic catalysts have to be considered when designing and fabricating high performance bimetallic catalysts. The experimental results confirmed this inference.

According to dechlorination efficiencies of the as-prepared Pd–Fe bimetallic catalysts listed in Table 1, dechlorination activity of the Pd–Fe catalysts first increases and then decreases with the decrease of Pd/Fe weight ratio. At the weight ratio of 5.9, the bimetallic catalyst exhibits the highest dechlorination activity (97.4%) under otherwise identical conditions (temperature: 303 K; electrolysis time at −0.2 V: 30 min). When the Pd/Fe weight ratio is much larger than 5.9 (e.g. 399), Fe components are either passivated due to serious galvanic corrosion or prevented by the Pd components from contacting aqueous solutions. The aforementioned two factors decrease the amount of atomic hydrogen adsorbed on the Pd components, thereby leading to the relatively low dechlorination efficiency (84%). On the contrary, when the Pd/Fe weight ratio is lower than 5.9 (e.g. 4.9 and 0.2), the catalytic active sites available for chemisorption of CT and hydrogen are evidently reduced. Moreover, the corrosion rate of Fe components is decreased as the area of cathodic metal (Pd) is decreased. It is unsurprising that the dechlorination efficiency of CT over the bimetallic catalysts with low Pd/Fe weight ratios become much lower (51.9% for Pd/Fe ratio: 4.9 and 40.7% for Pd/Fe ratio: 0.2).

3.3.3. Effect of temperature

Taking electrochemical reductive dechlorination of CT on the Pd–Fe thin films (Pd/Fe ratio: 5.9) as an example, we studied the influence of temperature on the rate of CT dechlorination at a constant potential of −0.2 V. Increasing temperature has a beneficial influence on the CT dechlorination. The removal efficiency of CT increased from 92.4% to 97.4%, 98.1% and nearly complete removal (99.9%) as the temperature gradually increased from 298 K to 303 K, 313 K and 323 K.

The effect of temperature was also used to evaluate the activation energy of CT dechlorination reaction on the Pd–Fe thin films. The electrode reaction rate can be defined in term of current density and activation energy, as shown in Eq. (4).

$$\left(\frac{\partial \ln I}{\partial T}\right)_{\eta} = -\frac{E_a}{RT^2} \quad (4)$$

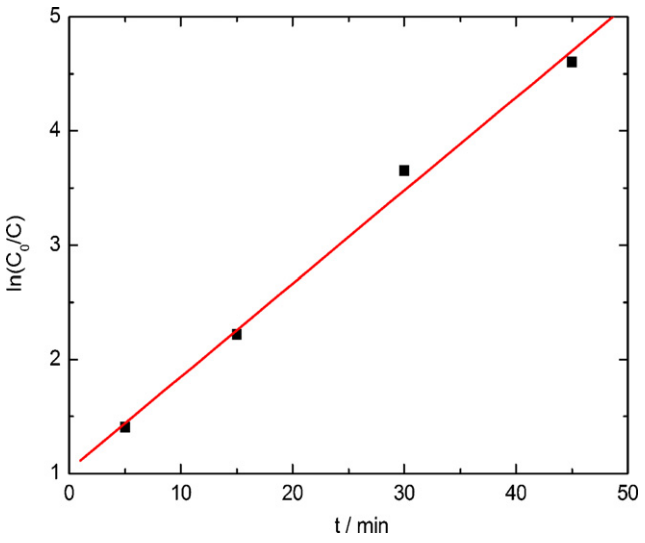

Fig. 5. Relationship between $\ln(C_0/C)$ and reaction time (t).

where η is overpotential, E_a is activation energy, R is the gas constant, and T is the absolute temperature. Integrating Eq. (4) results in:

$$\ln I = -\frac{E_a}{RT} + \ln A \quad (5)$$

where A is an integral constant. Thus, plotting $\ln I$ against $1/T$ creates a set of Arrhenius plots for the CT dechlorination reaction. Based on the relationship between $\ln I$ and $1/T$, the E_a values under different cathodic potentials were calculated and listed in Table 2. It is found that the E_a value is the lowest at −0.2 V, and the highest at −0.15 V.

3.3.4. Effect of electrolysis time

Due to the higher dechlorination activity, the bimetallic Pd–Fe catalyst with Pd/Fe weight ratio of 5.9 was selected to investigate the dependence of dechlorination efficiency on the reaction time at a given potential (−0.2 V) and temperature (303 K). The concentration of CT in the solutions decreased with the prolonged electrolysis time, which in turn increased the dechlorination efficiency of CT. The dechlorination efficiency increased evidently with electrolysis time and reached 99% after reaction for 45 min. In particular, CH_4 is the leading product [32]. Furthermore, after 10 successive measurements, the steady state current for electrochemical dechlorination was decreased by ~27.3%, which indicates a relatively high stability of the as-prepared Pd–Fe bimetallic films during electrochemical reductive dechlorination of CT.

Previous studies have shown that the degradation of CT is a pseudo-first-order reaction [32–36]. The kinetics equation of the reaction process can be expressed in Eq. (6).

$$\frac{dc}{dt} = -k_{obs}C \quad (6)$$

where k_{obs} is the apparent first-order rate constant, and C denotes the transient concentration of CT during the reaction process.The integration of Eq. (6) results in:

$$\ln \frac{C_0}{C} = k_{obs}t \quad (7)$$

where C_0 is the initial CT concentration and t stands for electrolysis time.

The natural logarithm of C_0/C as a function of time for CT degradation is shown in Fig. 5 (with a regression coefficient of 0.997). The logarithmic plot versus time is linear, whose slope is equal to k_{obs}. The apparent first-order rate constant k_{obs} for CT dechlorination reaction are 8.15×10^{-2} min^{-1}. The lager k_{obs} (compared to the previous reported values [34]) demonstrates that our as-prepared Pd–Fe bimetallic film electrode is an effective catalyst for CT dechlorination reaction.

4. Conclusions

Nanostructured Pd–Fe bimetallic thin films were directly fabricated on glassy carbon substrates by means of double-potential step electrodeposition and galvanic replacement methods. The Pd/Fe weight ratio in the bimetallic films is an important parameter that affects the dechlorination activity of the bimetallic catalysts and can be adjusted by selecting nanostructured Fe film templates with different thickness and surface morphology, which are dependent on the concentration of Fe^{2+} ions in electrolyte solutions. When the weight ratio of Pd/Fe is 5.9, the bimetallic thin film catalyst exhibits the highest dechlorination activity. The activation energy E_a for dechlorination by different types of hydrogen is in accord with the removal efficiency of CT, and a minimum E_a and the highest removal efficiency were obtained at −0.2 V. Besides, the removal efficiency of CT increased considerably with increasing temperature. The reaction was found to be pseudo-first-order.

Acknowledgements

This work was supported by National Natural Science Foundation of China (21073111), Beijing National Laboratory for Molecular Science, and the National Basic Research Program of China (2009CB930103).

References

[1] D. Wei, T. Kameya, K. Urano, Environ. Int. 33 (2007) 894–902.
[2] W.K. Chu, M.H. Wong, J. Zhang, Environ. Geochem. Health 28 (2006) 169–181.
[3] R.E. Doherty, J. Environ. Forensics 1 (2000) 69–81.
[4] B.R. Helland, P.J.J. Alvarez, J.L. Schnoor, J. Hazard. Mater. 41 (1995) 205–216.
[5] V. Janda, P. Vasek, J. Bizova, Z. Belohlav, Chemosphere 54 (2004) 917–925.
[6] B.W. Zhu, T.T. Lim, J. Feng, Chemosphere 65 (2006) 1137–1145.
[7] H.L. Lien, W.X. Zhang, Appl. Catal. B: Environ. 77 (2007) 110–116.
[8] Z. Sun, B. Li, X. Hu, M. Shi, Q. Hou, Y. Peng, J. Environ. Sci. 20 (2008) 268–272.
[9] L.J. Matheson, P.G. Tratnyek, Environ. Sci. Technol. 28 (1994) 2045–2053.
[10] W.X. Zhang, J. Nanopart. Res. 5 (2003) 323–332.
[11] W.X. Zhang, C.B. Wang, H.L. Lien, Catal. Today 40 (1998) 387–395.
[12] X.Y. Wang, C. Chen, H.L. Liu, J. Ma, Ind. Eng. Chem. Res. 47 (2008) 8645–8651.
[13] C. Grittini, M. Malcomson, Q. Fernando, N. Korte, Environ. Sci. Technol. 29 (1995) 2898–2900.
[14] J. Xu, A. Dozier, D. Bhattacharyya, J. Nanopart. Res. 7 (2005) 449–467.
[15] B. Schrick, A.D. Blough, J.L. Jones, T.E. Mallouk, Chem. Mater 14 (2002) 5140–5147.
[16] L.H. Chen, C.C. Huang, H.L. Lien, Chemosphere 73 (2008) 692–697.
[17] C.J. Lin, S.L. Lo, Y.H. Liou, J. Hazard. Mater. 116 (2004) 219–228.
[18] G.V. Lowry, M. Reinhard, Environ. Sci. Technol. 35 (2001) 696–702.
[19] S. Gómez-Quero, F. Cárdenas-Lizana, M.A. Keane, Ind. Eng. Chem. Res. 47 (2008) 6841–6853.
[20] L.M. Gómez-Sainero, X.L. Seoane, A. Arcoya, Appl. Catal. B: Environ. 53 (2004) 101–110.
[21] Y.H. Kim, E.R. Carraway, Environ. Technol. 249 (2003) 69–75.
[22] J. Choi, K. Choi, W. Lee, J. Hazard. Mater. 162 (2009) 1151–1158.
[23] Y.X. Chen, S.P. Chen, Q.S. Chen, Z.Y. Zhou, S.G. Sun, Electrochim. Acta 53 (2008) 6938–6943.
[24] D. Grujicic, B. Pesic, Electrochim. Acta 50 (2005) 4405–4418.
[25] Y.-X. Chen, S.-P. Chen, Z.-Y. Zhou, N. Tian, Y.-X. Jiang, S.-G. Sun, Y. Ding, Z.L. Wang, J. Am. Chem. Soc. 131 (2009) 10860–10862.
[26] R. Woods, Chemisorption at electrodes. Hydrogen and oxygen on noble metals and their alloys, in: A.J. Bard (Ed.), Electroanalytic Chemistry: A Series of Advances, vol. 9, Marcel Dekker, New York, 1976, pp. 49–117.
[27] Y.L. Jiao, D.L. Wu, H.Y. Ma, C.C. Qiu, J.T. Zhang, L.M. Ma, Electrochem. Commun. 10 (2008) 1474–1477.
[28] Y.-H. Shih, Y.-C. Chen, M.-Y. Chen, Y.-T. Tai, C.-P. Tso, Colloids Surf. A: Physicochem. Eng. Aspects 332 (2009) 84–89.
[29] H. Choi, S.R. Al-Abed, S. Agarwal, D.D. Dionysiou, Chem. Mater. 20 (2008) 3649–3655.

[30] Y.L. Jiao, C.C. Qiu, L.H. Huang, K.X. Wu, H.Y. Ma, S.H. Chen, L.M. Ma, D.L. Wu, Appl. Catal. B: Environ. 91 (2009) 434–440.
[31] P.N. Bartlett, B. Gollas, S. Guerin, J. Marwan, Phys. Chem. Chem. Phys. 4 (2002) 3835–3842.
[32] T. Li, J. Farrell, Environ. Sci. Technol. 34 (2000) 173–179.
[33] J. Feng, T.-T. Lim, Chemosphere 66 (2007) 1765–1774.
[34] X.Y. Wang, C. Chen, Y. Chang, H.L. Liu, J. Hazard. Mater. 161 (2009) 815–823.
[35] Y.-H. Kim, E.R. Carraway, Environ. Sci. Technol. 34 (2000) 2014–2017.
[36] G.V. Lowry, M. Reinhard, Environ. Sci. Technol. 33 (1999) 1905–1910.